ACS OMEGA

http://pubs.acs.org/journal/acsodf

Article

New Model for Absolute Permeability Prediction in Coal Samples: Application of Modified Purcell Model to Mercury Injection Pressure and Nuclear Magnetic Resonance Data

Yanhai Chang, Kun Zhang,* and Yipeng Zhang

Cite This: *ACS Omega* 2023, 8, 21120−21132

Read Online

ACCESS | Metrics & More | Article Recommendations

ABSTRACT: The permeability of rocks is a critical parameter in many subsurface geological applications, and pore properties measured on rock samples (including rock fragments) can be used to estimate rock permeability. A major use of MIP and NMR data is to assess the pore properties of a rock in order to estimate the permeability based on empirical equations. Although sandstones have been extensively studied, permeability in coals has received less attention. Consequently, in order to obtain reliable predictions for coal permeability, a comprehensive study of different permeability models was performed on coal samples having a range of permeabilities from 0.003 to 1.26 mD. The model results showed that the seepage pores in coals account for the bulk of the permeability, while the contribution of adsorption pores to permeability is negligible. The models that only consider a single pore size point on the mercury curve, such as the Pittman and Swanson model, or those that use the entire pore size distribution, like the Purcell and SDR model, are inadequate for predicting permeability in coals. This study modifies the Purcell model to determine permeability from the seepage pores of coal, resulting in the enhancement of the predictive capability, with an increased R^2 and reduction in the average absolute error by approximately 50% compared to the Purcell model. To apply the modified Purcell model to NMR data, a new model was developed that provides a high degree of predictive capability (∼0.1 mD). This new model can be used for cuttings, which could lead to a new method for field permeability estimation.

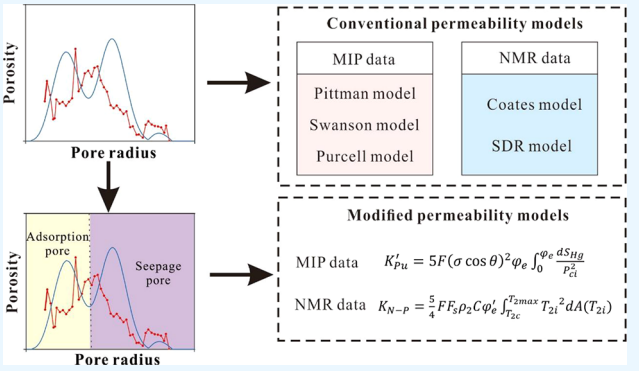

1. INTRODUCTION

Permeability is a crucial parameter for the production of coalbed methane reservoirs since it directly impacts the fluid flow and gas delivery. Well testing, core analysis, and well logging are the most common methods to measure reservoir rock permeability. However, all these methods are expensive and time-consuming, so there is a need for cheap and effective alternatives for estimating rock permeability.[1,2] Since the pore structure is commonly thought to influence the permeability through pore size distribution (PSD) and pore connectivity,[3−5] predicting permeability by means of correlations to pore structure parameters has gained prominence in formation evaluation, particularly in unconventional reservoirs with extremely complicated pore structures. Nuclear magnetic resonance (NMR) and mercury injection porosimetry (MIP) are two commonly used methods for assessing the pore characteristics of porous media, and both of them can be performed on cutting samples.[6] Also being inexpensive, cuttings are generally available throughout the length of the well bore, which may also make possible the evaluation of permeability in the field. Numerous permeability prediction models have been developed on the basis of MIP and NMR parameters. The Swanson model, Pittman model, and Purcell model, for instance, are based on relationships between permeability and pore parameters determined by MIP, while the Schlumberger-Doll Research (SDR) and Coates model use the NMR data.[4−7]

Since these permeability prediction models were developed for conventional sandstones and carbonates,[8,9] applying these models directly to coals with different physical and petrophysical properties represents special challenges.[4,10] In particular, MIP has limitations when probing coal pore structures due to the influence of interparticle voids and coal compression.[11−13] Because of the resulting inaccuracies in the pore structure characterization, inaccurate pore structure

Received: March 28, 2023
Accepted: May 9, 2023
Published: June 2, 2023

Table 1. Permeability Prediction Models that Incorporate MIP and NMR Data

method	advantages	disadvantages	references
Pittman model	considers the effect of porosity	focuses on a single pore size value from the capillary pressure curve; uncertainty in the choice of the pore throat size; lack of theoretical basis	4,19,20,49
Swanson method	reliable permeability prediction for high-permeability sandstones and carbonates	unsuitable for low-permeability reservoir; does not consider the porosity; lack of theoretical basis	8,24
Purcell model	has a theoretical basis; relates the permeability to a wide PSD	overestimates the contribution of micropores to permeability	7,29
SDR model	reliable permeability prediction for sandstone; available at the borehole	sensitive to the fluid in the pores; considers the total porosity; lack of theoretical basis	30,31
Coates model	reliable permeability prediction for sandstone; available at the borehole; uses the connectivity porosity	lack of theoretical basis; requires a cutoff value for of T_2	16,35

parameters are frequently determined, resulting in errors in permeability estimation.[14−18] A key advantage of NMR is that it can overcome the potential deficiencies of MIP in measuring the pore structure of coal. However, the widely used models, such as the Coates model and the SDR model, are empirically derived for sandstones, and their application to the prediction of coal permeability is debatable.[17] In light of these issues, the main objective of this study is to develop a reliable permeability estimation model for coal that takes into account pore structure constraints. A set of coal samples with a variation of permeability over three orders of magnitude were collected from the Qinshui Basin, Ordos Basin, and Junggar Basin of China for this study. An analysis of different permeability prediction models using MIP and NMR data was conducted, and a reliable permeability estimation model for coals constrained by pore connectivity was developed.

2. REVIEW OF PERMEABILITY PREDICTION MODELS

The commonly used permeability estimation models are summarized in Table 1, of which the Coates and SDR models use NMR data, while the Pittman model, Swanson model, and Purcell model use MIP parameters.

(1) Pittman model. Porosity, permeability, and r_{35} (throat size that corresponds to a mercury saturation of 35%) were empirically related by Kolodzie.[18] Based on a multiple regression analysis method, Pittman further studied the correlation between porosity, air permeability, and other parameters from MIP data, and found that r_{20} and r_{25} were the most robust parameters for the estimation of sandstone permeability.[19] Subsequently, additional work has shown that r_{50} and r_{55} are also effective parameters for permeability prediction of sandstone.[20,21] The Pittman model has also been applied to other reservoir rocks, in which the r_{10} was suggested for tight sandstone[4] and r_{20} for carbonate rocks.[22] All these models can be described as follows:

$$\log K_P = C_P + \alpha_P \log \varphi + \beta_P \log r_i \quad (1)$$

where K_P is the absolute permeability; mD; C_{M1}, α_{M1}, and β_{M1} are empirical constants, φ is the helium porosity, %, and r_i is the pore radius corresponding to i percentage of cumulative mercury saturation, μm. Porosity and pore radius are the two main variables in the Pittman model that greatly influence the permeability prediction. However, Liu et al. pointed out that the Pittman model relied on only one point of the MIP curve to estimate permeability, which may cause large errors in permeability prediction.[23]

(2) Swanson model. Swanson found that the maximum ratio of mercury injection saturation to capillary pressure (i.e., Swanson's parameter, $\left(\frac{S_{Hg}}{P_c}\right)_A$) corresponds to the apex of the hyperbola, which is the maximum filling of effectively interconnected pore spaces with mercury.[6] Based on extensive experiments, Swanson developed the empirical equation for the Swanson's parameter and permeability of sandstone and carbonate, which is expressed as

$$K_S = \alpha_S \left(\frac{S_{Hg}}{P_c}\right)_A^{\beta_S} \quad (2)$$

where K_S is the absolute permeability, mD; S_{Hg} is the saturation of mercury intrusion, %; P_c is the pressure of mercury intrusion, MPa; $\left(\frac{S_{Hg}}{P_c}\right)_A$ is the Swanson's parameter, MP; and α_S and β_S are the empirical constants. The Swanson model has been widely used for the permeability prediction of normal sandstones and carbonates.[24−26] However, studies have also shown that the Swanson model is ineffective for low-permeability tight sandstones and carbonates.[27,28]

(3) Purcell model. By combining the Washburn equation, Darcy's law, and Poiseuille's law, Purcell developed a model for calculating the absolute permeability of porous media, which assumes parallel cylindrical capillaries with different radii but similar lengths.[7] The Purcell model is

$$K_{Pu} = 5F(\sigma\cos\theta)^2 \varphi \int_0^1 \frac{dS_{Hg}}{P_{ci}^2} \quad (3)$$

where K_{Pu} is the permeability, mD; F is the dimensionless lithology factor; σ is the interfacial tension (0.48 N/m for mercury−air system); θ is contact angle, 140°; S_{Hg} is the dimensionless ratio of mercury volume to pores volume; φ is the helium porosity, in percent; and P_{ci} the capillary pressure, MPa. Since it relies more on theoretical relationships than on empirical ones that use only one point on the mercury curve, the Purcell model relates the permeability of porous media to the entire PSD. However, according to Zhang and Weller,[29] the Purcell model is problematic for estimating permeability because small pores do not contribute to permeability.

(4) The SDR model: A general description of the SDR model is as follows:[30]

$$K_{SDR} = C_{SDR} T_{2g}^{\alpha_{SDR}} \varphi_{NMR}^{\beta_{SDR}} \quad (4)$$

where T_{2g} is the geometric mean of T_2 distribution, ms; φ_{NMR} is the NMR porosity, %; and C_{SDR}, α_{SDR}, and β_{SDR} are the empirical parameters of the SDR model. Previous work has shown that reasonable permeability estimates can be made for sandstones by using constant coefficients in the SDR model.[31−34] Maclean et al. suggested that the SDR model is accurate for permeability estimation of sandstones because sandstone grain sorting is regular, and the porosity is mainly

https://doi.org/10.1021/acsomega.3c02035
ACS Omega 2023, 8, 21120−21132

Table 2. Maceral Compositions, Proximate Analysis, Porosity, and Permeability of the Core Samples[a]

		maceral composition (%)				proximate analysis (%)					
sample	R_o (%)	V	I	L	M	M_{ad}	A_d	V_d	FC_d	φ (%)	K (mD)
S1	2.88	86	11	0	3	1.5	4.7	6.2	89.0	7.8	0.003
S2	3.35	80	16	0	T	2.1	11.6	6.8	81.7	9.0	0.068
S3	3.25	73	22	0	5	2.1	11.3	7.1	81.6	8.6	0.011
S4	0.47	68	20	9	3	1.9	10.6	20.6	68.6	10.5	1.260
S5	0.84	30	67	T	T	7.7	21.3	26.7	44.9	14.8	0.995
S6	0.73	45	32	T	23	2.5	23.0	37.8	39.2	4.2	0.443

[a]*Notes*: M_{ad}, moisture content (air-dried basis); A_d, ash yield (dry basis); V_d, volatile matter yield (dry, ash-free basis); FC_d, fixed carbon content (air-dried basis). V, vitrinite; I, inertinite; L, liptinite; M, minerals; T, trace; φ, He gas porosity; K, gas permeability.

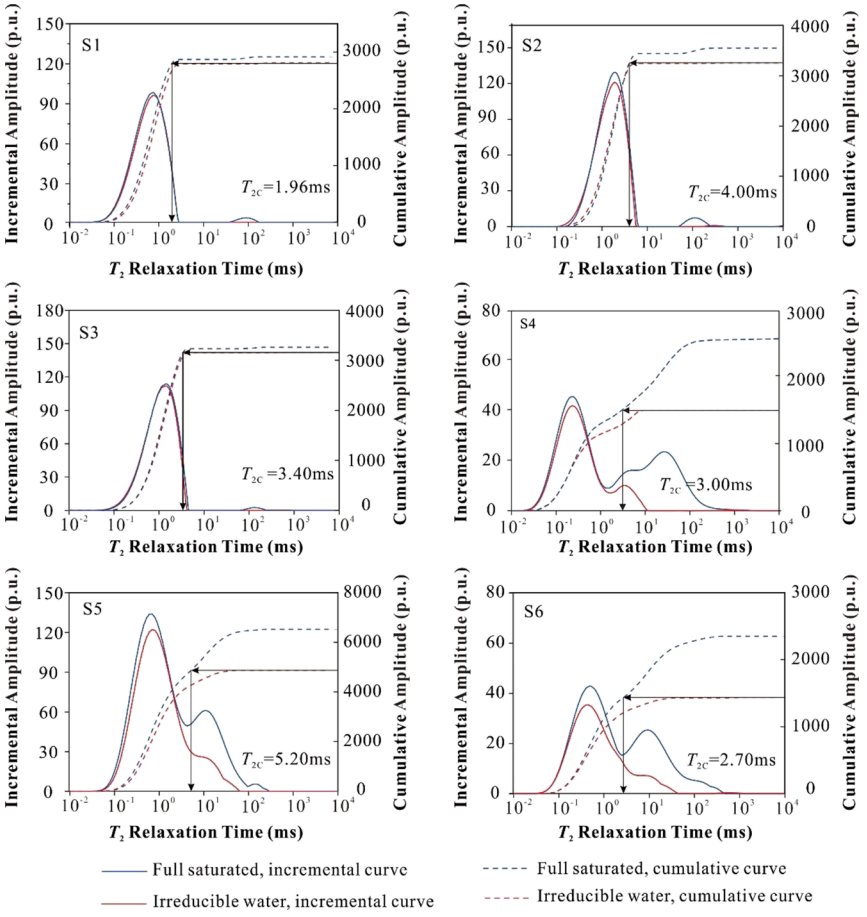

Figure 1. NMR measurements at full water-saturated condition (S_w) and at irreducible water condition (S_{ir}) as well as the method to calculate a T_2 cutoff value (T_{2c}). The labels S1−S6 denote the identification of the samples.

intergranular, but that the equation is less precise in carbonates because of complex pore types.[35] In addition, Xiao et al. pointed out that the SDR model cannot predict the permeability of tight sandstone because of the poor relationship between permeability and T_{2g}.[28]

(5) The Coates model is expressed as follows:[32]

$$K_C = \left[\left(\frac{\varphi_{NMR}}{C_C}\right)^{\alpha_C} \frac{FFI}{BVI}\right]^{\beta_C} \quad (5)$$

where K_C is absolute permeability, mD; $\frac{FFI}{BVI}$ is the ratio of the free fluid part (FFI) to the bound fluid part (BVI). This ratio is determined by the T_{2c} (the cutoff value T_2 that divides the T_2 distribution into the irreducible fluid (bound fluid) and movable fluid (free fluid)). C_{N1}, α_{N1}, and β_{N2} are the empirical parameters of the Coates model, which vary in different study areas and rocks. The model has demonstrated good predictability for sandstone permeability. However, since capillary-bound water cannot be centrifuged completely for tight sandstone, the $\frac{FFI}{BVI}$ cannot adequately describe fluid mobility, which can cause poor permeability prediction.[16,36]

In conclusion, since all of these permeability prediction models are based on conventional sandstone properties, there are problems when they are applied directly to rocks with heterogeneous pore structures such as tight rocks and coals. For this reason, the applicability of these models to predict the permeability of coal needs to be further improved.

https://doi.org/10.1021/acsomega.3c02035
ACS Omega 2023, 8, 21120−21132

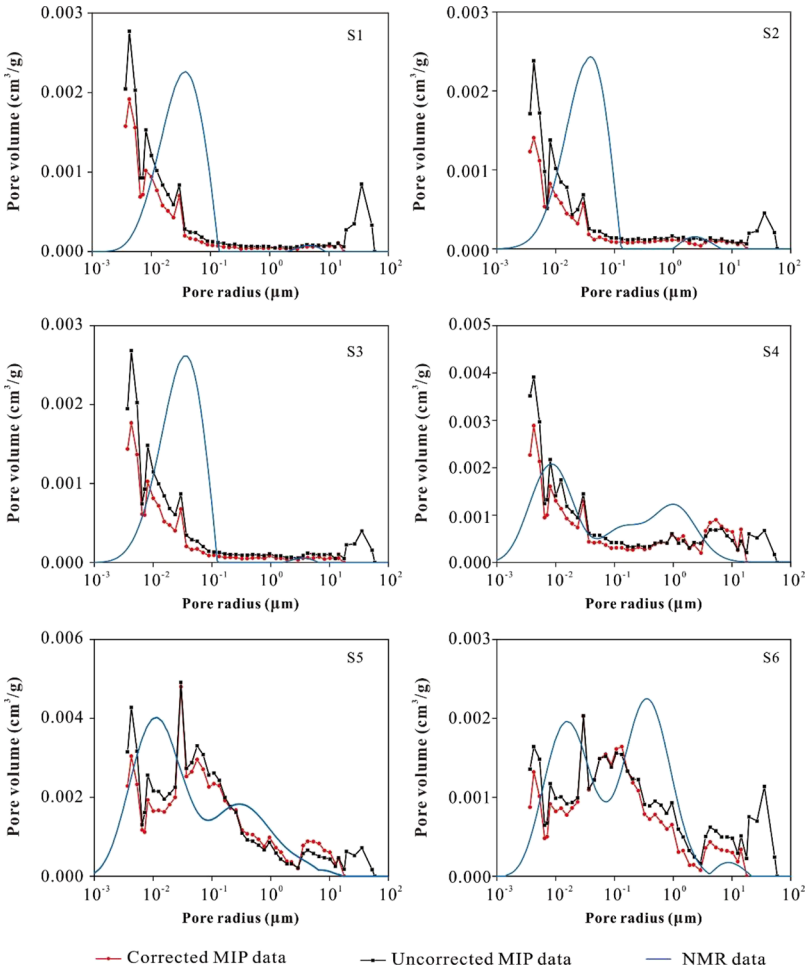

Figure 2. The PSD of NMR data, MIP data, and corrected MIP data. The labels S1−S6 denote the identification of the samples.

3. SAMPLES AND EXPERIMENTS

3.1. Samples. Six coal samples with varying permeabilities were chosen for comparison of different models for predicting permeability. The sample compositional data are contained in Table 2. The selected samples include high volatile bituminous coals, medium volatile coals, and anthracite coals with a maturity range of R_o = 0.47−3.35%. The coals were taken from the Qinshui Basin, Ordos Basin, and Junggar Basin of China. The samples in this study are all cylindrical in shape and cut parallel to the bedding direction, with diameters of 25 mm and lengths of 50 mm.

According to the maceral composition analysis (Table 2), the major components are vitrinite (30−86%), inertinite (11−67%), and liptinite (<10%). The mineral contents are generally <5% except for sample S6, which has a mineral concentration of 23%. The proximate analysis shows that the moisture content is 1.5−7.7%, ash yield ranges from 4.7−23.0%, volatile matter yield is 6.2−37.8%, and fixed carbon content varies from 44.9−89.0%. Helium porosimetry and core permeability analysis methods were used to measure porosity and absolute air permeability. Table 2 contains the maceral compositions, proximate analysis, porosity, and permeability of the samples.

3.2. Experimental Methods. For all six samples, MIP and NMR experiments were performed in this study. Following Chinese Oil and Gas Industry Standard SY/T 5346−2005, the MIP experiments were performed with a 9520 Automatic mercury porosimeter, which has a pressure of up to 200 MPa. The Oxford GeoSpec 12/53 instrument was used for the NMR studies. A typical Carr-Purcell-Meiboom-Gill (CPMG) NMR pulse sequence was used to calculate the transverse relaxation time T_2.[14] The signal-to-noise ratio was increased to 200 by setting the NMR measurement parameters as follows: echo spacing of 0.132 ms, recycling delay of 750 ms, and echo numbers of 3788. The NMR measurements on the core plugs were first conducted at 100% water saturation. Subsequently, the samples were centrifuged in a PC-1 Petroleum Core Centrifuge to obtain the irreducible water saturation condition (i.e., the minimum water saturation achievable by the centrifuge), after which the samples were again analyzed.

4. RESULTS

4.1. NMR Results. *4.1.1. NMR T_2 Distribution.* The NMR T_2 spectra acquired at 100% water-saturated condition (S_w) and irreducible water condition (S_{ir}) are displayed in Figure 1. The T_2 values of coals commonly show wide relaxation time distributions, ranging from 0.1 to 1000 ms. The selected coals contain typical bimodal or trimodal distribution. The coal samples with permeability <0.1 mD are characterized by bimodal distributions, with peaks located at 0.1−10 ms and 50−200 ms. The left (lower value) peak contains more than 90% of the total peak areas, indicating the dominant contribution of small pores to porosity (samples S1, S2, and S3). The coal samples with permeability >0.1 mD exhibit trimodal distributions (samples S4, S5, and S6). Compared to

https://doi.org/10.1021/acsomega.3c02035
ACS Omega 2023, 8, 21120−21132

the bimodal distribution, the third peak is in the interval of 1−100 ms, and the peak at >100 ms is increased in size, indicating increased contributions of larger pores in permeability.

By definition, the T_2 cutoff value (T_{2c}) separates the movable and irreducible fluid porosity in the T_2 spectrum of NMR. The T_{2c} of coal can be acquired from accumulative T_2 spectra at saturated and irreducible water conditions,[35] as shown in Figure 1. The irreducible fluids are mainly trapped in adsorption pores, where fluid cannot be easily drained due to capillary pressure, while the movable fluids are stored in seepage pores where they can be easily drained by centrifugation. The T_{2c} values for these six coal samples range from 1.96 to 5.2 ms (Figure 1), which is similar to the values of 2−31 ms published by Yao et al.[16] Generally, the coal samples with high permeability exhibit high movable fluid contents, and low-permeability samples exhibit high irreducible fluid contents, which indicates that seepage pores contribute to the bulk of the permeability of coals.

4.1.2. PSD Determination from NMR Data. Previous studies have shown that T_2 is linear with the pore size,[17,20,35,37] which can be determined from the centrifuge-T_{2c} method.[14] Consequently, the PSD can be generated from the T_2 spectra. By using this method (detailed in references of Yao et al.[16] and Zheng et al.[37]), the T_2 spectra of coal samples in this study are converted into the PSDs.

Figure 2 shows the PSD determined from the NMR data. The low-permeability samples (S1, S2, and S3) are dominated by the small pores (<0.1 μm). In contrast, the large pores (>0.1 μm) are responsible for the high permeability of samples S4, S5, and S6. The comparison of the PSD determined by NMR with that determined by MIP is described in detail in Section 4.2.2.

4.2. MIP Results. *4.2.1. Original MIP Results.* In Figure 3, raw mercury intrusion and extrusion profiles for the six coal

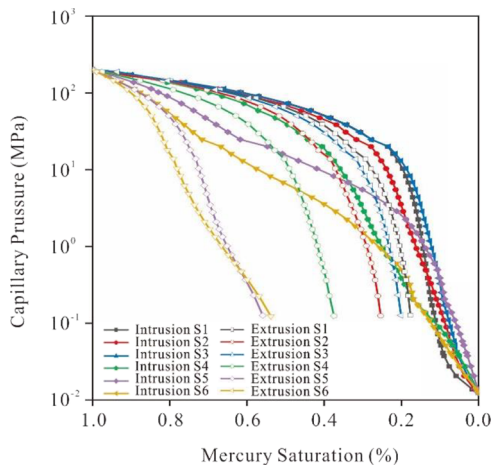

Figure 3. Mercury intrusion−extrusion curves of the samples.

samples are shown. Despite the differences in coal rank, all samples showed noticeable increases in intruded mercury volumes at high pressure, while a slight increase in mercury volume at low pressure. However, it remains unclear whether all the intruded mercury can be attributed only to the pore volume of coal. Coal is an elastic organic rock, and under high injection pressure, the matrix is easily compressed mechanically.[14] Due to the loose packing of coal particles, the mercury can enter the interparticle voids first at low injection pressure.[13] Consequently, the intruded mercury volume should equal the sum of interparticle voids filling, intraparticle pore filling, and matrix compression. Consequently, the pore volume is expected to be overestimated based on the original MIP data. Before using MIP results to characterize the pore structures of coals, the effects of interparticle voids and coal compressibility should be carefully examined and corrected.

Fractal theory is a powerful analytical tool that has been widely applied to represent the pore structure of coals.[38,39] It has also been demonstrated that the fractal dimensions of porous solids can also be used as a "fingerprint" to distinguish interparticle voids filling, intrapore filling, and matrix compression for MIP data.[12,40,41] Based on Li's fractal model (i.e., $S_{Hg} = aP_c^{D-2}$), the fractal dimension (D) can be obtained by plotting S_{Hg} and P_c on a logarithmic plot.[42] Figure 4 shows the calculation of fractal dimension for the six coal samples, and the curves are divided into three fractal domains ($D1$, $D2$, $D3$) by two inflections. The pressure corresponding to these two inflections is called the threshold pressure (P_t) and upper limit pressure (P_u) (Figure 4). P_t is close to 0.03 MPa and P_u is close to 30 MPa for all samples.

At the low pressure range ($P < P_t$), the fractal dimensions ($D1$) are larger than 3 for all samples, which means the space where mercury enters at $<P_t$ is not fractal because intergranular voids are not fractal,[43] implying that interparticle voids are predominant in filling mercury at $<P_t$. Actually the interparticle voids mainly depend on the sample size but have nothing to do with coal composition.[13] For all six samples, the P_t acquired from the fractal method is close to 0.03 MPa. It is concluded that the process of interparticle void filling continued until the threshold pressure (P_t).

At the high pressure range ($P > P_u$), the coal matrix is compressed. Based on the fractal method, the previous work found that the upper limit pressure is around 30 MPa for different rank coals,[12,13] which agrees with these results. More importantly, a linear relationship between pressure and intrusion volume is a characteristic of coal compressibility at higher pressures.[12,44,45] In this study, the mercury intrusion volume as a function of pressure is presented in Figure 5. The curves can be separated into the linear region and nonlinear region at 30 MPa, supporting that coal compression is dominant in the high-pressure region.[46]

4.2.2. Correction of MIP Result. As discussed above, the MIP results of coal are inaccurate because of the coal compressibility and interparticle voids. In this section, we will correct the MIP results to obtain reliable data for the characterization of the coal pore structure.

With the increasing invasion pressure, the intruded mercury tends to fill the interparticle voids first, which may be misinterpreted as larger pores in coals. As discussed above, when $P < P_t$, mercury has not yet occupied the intrapore volume of the coal samples, and thus the data were removed from the MIP data for a reliable pore structure characterization. The correction model of coal compressibility proposed by Li et al.[11] has been successfully used to correct the MIP data of coal at high pressure.[41,47,48] The correction process consists of two steps: first, calculating the matrix compressibility coefficients of coal and second, correcting the mercury volume caused by matrix compression. The matrix compressibility coefficients were calculated to be 3.82×10^{-11}, 3.56×10^{-11}, 3.77×10^{-11}, 4.56×10^{-11}, 5.30×10^{-11}, and 1.53×10^{-11} N^{-1}

https://doi.org/10.1021/acsomega.3c02035
ACS Omega 2023, 8, 21120−21132

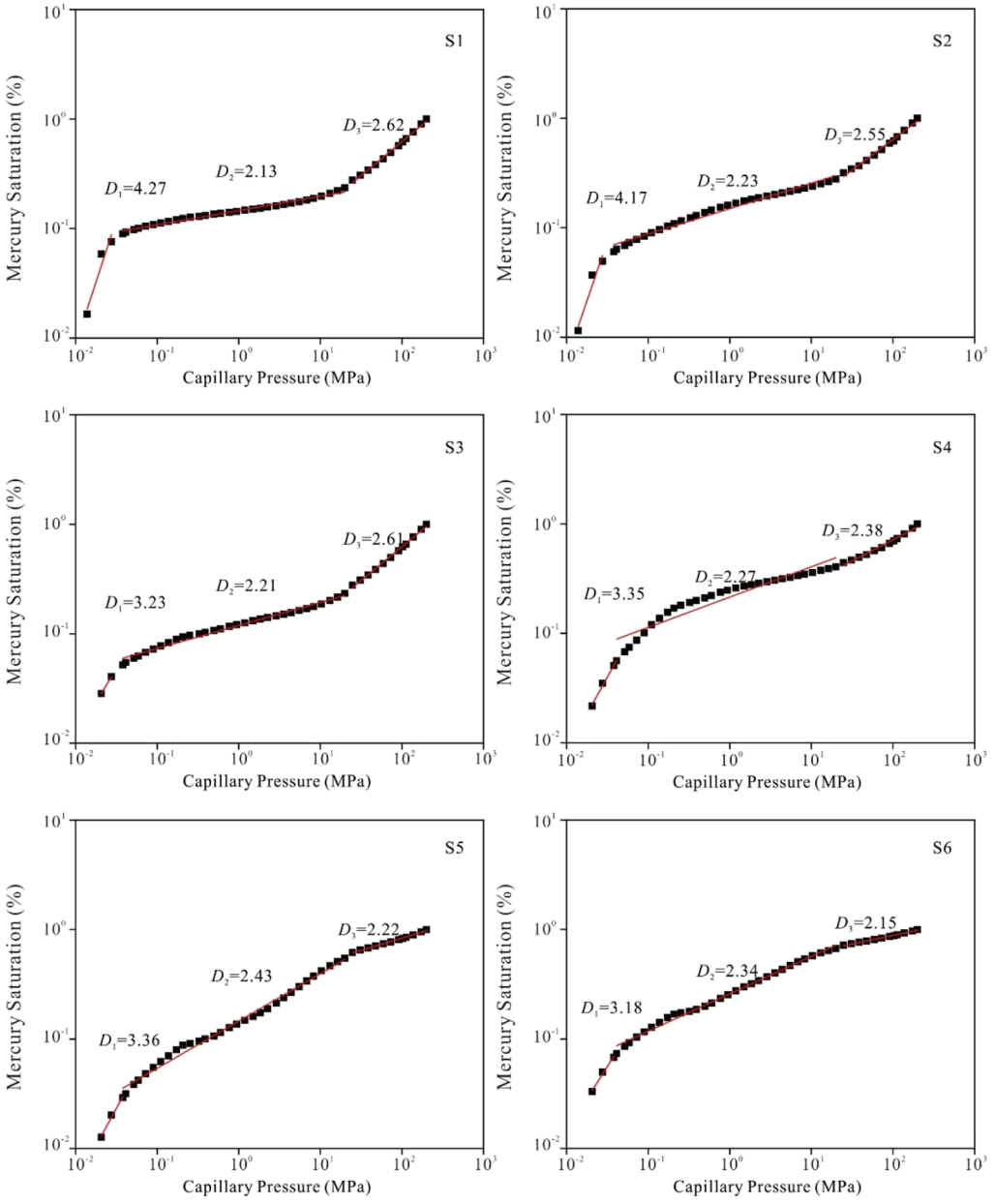

Figure 4. The straight lines are fitted to log P verses log S_{Hg} data to estimate fractal dimension (D). Fractal dimension values for different pore regions are shown on the graphs. The labels S1−S6 denote the identification of the samples.

for S1−S6, respectively, which is close to the value of 7×10^{-11} to 2.3×10^{-10} N^{-1} reported for coal by Toda and Toyoda.[45]

A comparison of mercury intrusion curves before and after correction for the interparticle voids and coal compressibility is shown in Figure 6. The corrected results are distinctly lower than those of raw data, indicating that the pore volume is overestimated by raw MIP data. When the PSD of MIP results before and after corrections was compared with the PSD derived from the NMR data (Figure 2), it can be seen that the PSD acquired via NMR and that via the corrected MIP data are in the same range of 0.001−10 μm, while that of raw MIP results has a wider pore size range (0.001 to 100 μm). This indicates that the interparticle voids are effectively removed by this correction method. However, it is unlikely that MIP and NMR measurements will coincide due to the physical differences between the two measurements (Figure 2). NMR data represent the distribution of the pore body radii, while MIP data reflect the throat radii.[29] Generally, the pore volume from MIP was lower than that obtained from NMR data. Due to the fact that MIP and NMR determine pore characteristics based on fluid intrusion, such as water and mercury. On one hand, the water molecule can enter a smaller pore than mercury. On the other hand, if some pores have nanometer-sized pore entrances, these pores may not be detected by mercury intrusion.[12]

5. DISCUSSION

5.1. Prediction of Permeability by Models. In this study, a comparison of the various permeability prediction models was conducted to investigate their applicability to permeability predictions for the coal samples. For MIP data, three permeability estimation models were investigated, including the Pittman, Swanson, and Purcell models, while

https://doi.org/10.1021/acsomega.3c02035
ACS Omega 2023, 8, 21120−21132

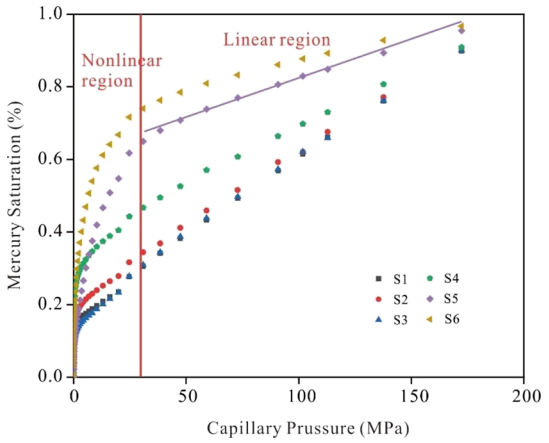

Figure 5. Linear region and nonlinear region of mercury intrusion volume as a function of pressure (red line is 30 MPa).

the SDR and Coates models were the model studied that used NMR data.

5.1.1. Pittman Model. The Pittman model is based upon the correlation between permeability, porosity, and pore radii at different mercury saturations.[19] Using the Pittman model, it was proposed in the previous work to use the r_{10}, r_{35}, r_{40}, and r_{50} to predict sandstone permeability.[2,20,49] In this study, the correlation between permeability and pore radii at a mercury saturation of 5, 10, 25, 35, 50, and 75% is plotted in Figure 7. The permeability shows no linear correlation with the pore radii at mercury saturation >25%. In contrast, a good correlation is observed between permeability and the radii at mercury saturation <25% with correlation coefficients (R^2) between 0.7937 and 0.8942. For mercury saturation <25%, mercury mainly enters the pores >0.1 μm (red dashed line in Figure 7). Conversely, mercury invades the pores <0.1 μm at mercury saturation >25%. This phenomenon suggests that the pores >0.1 μm are the main contributor to permeability in coals. In normal sandstones, the pore radii at mercury saturation >35% (r_{35}*or* r_{55}) are the best indicator of permeability.[19] For tight sandstone with a complex pore structure, Rezaee et al. found the correlation coefficients between permeability and pore throat radii at r_5-r_{25} are >0.70, while no obvious correlation is found between permeability and pore throat radii at saturations of $r_{25}-r_{80}$.[20] Because coal and tight sandstone contain complex pores that are generally poorly connected, they behave differently from normal sandstone. Rezaee et al. chose r_{10} as the best permeability predictor for tight sandstone because the correlation of permeability and pore radii was the best at that level.[20] However, a flaw in this methodology is that that many pores

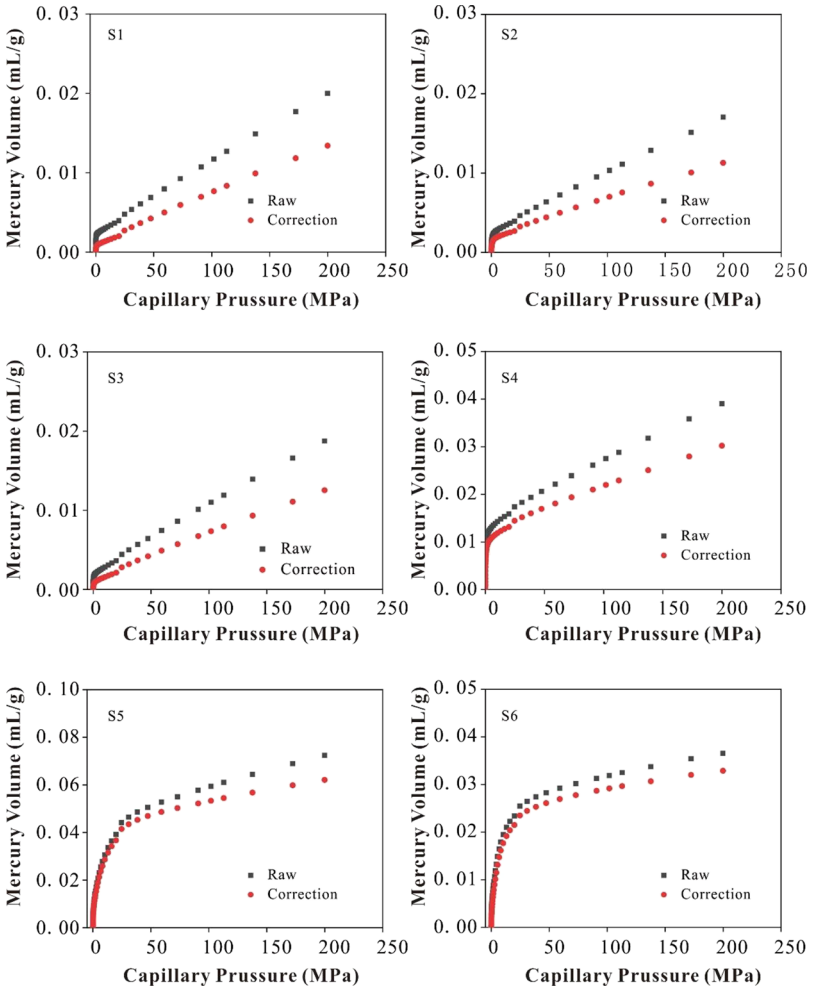

Figure 6. The mercury intrusion data before and after corrections of the interparticle void and coal compressibility. The labels S1−S6 denote the identification of the samples.

https://doi.org/10.1021/acsomega.3c02035
ACS Omega 2023, 8, 21120−21132

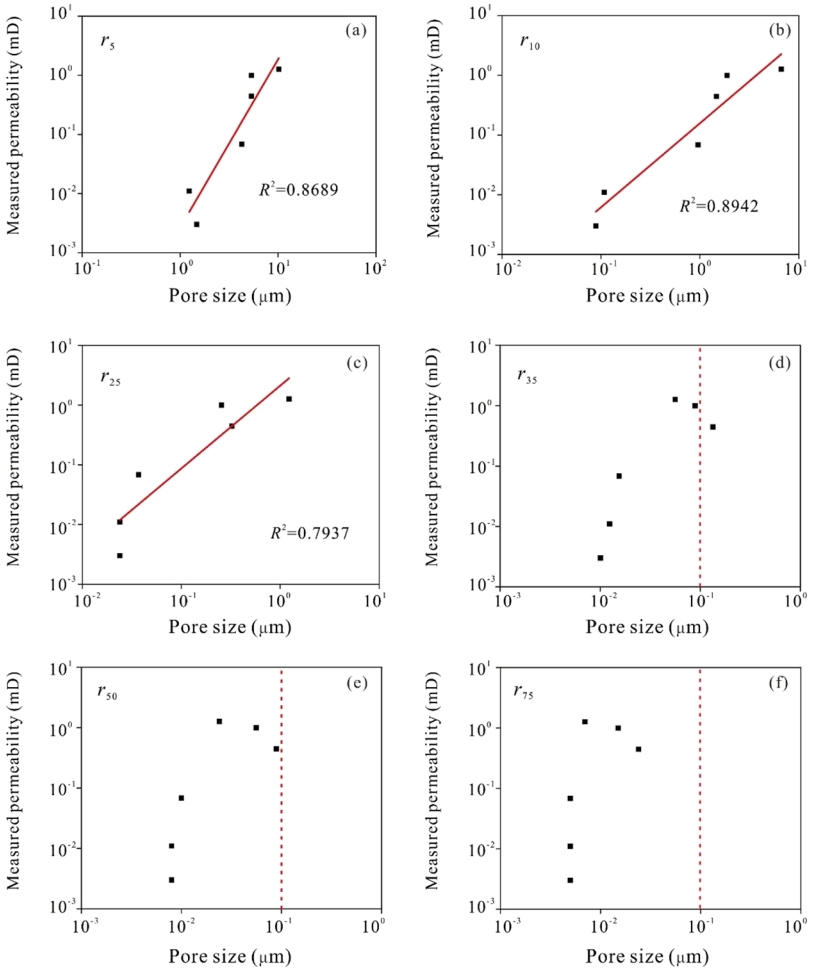

Figure 7. Relationship between the pore sizes at mercury saturation levels of 5% (a), 10% (b), 25% (c), 35% (d), 50% (e), and 75% (f) versus permeability in the log−log coordinate. The red dashed line corresponds to the pore size of 0.1 μm.

contributing to permeability are neglected if only one level of mercury saturation (i.e., one pore radii) is selected.

5.1.2. Swanson Model. As shown in eq. 2, the Swanson's parameter is correlated with permeability. The Swanson's parameter is the maximum ratio of mercury injection saturation to capillary pressure ($\left(\frac{S_{Hg}}{P_c}\right)_A$), which corresponds to the maximum filling of effectively interconnected pore spaces with mercury.[6] Equation 2 can be simplified as follows:

$$\log K_S = \log \alpha_S + \beta_S \log\left(\frac{S_{Hg}}{P_c}\right)_A \quad (6)$$

As shown in Figure 8, the Swanson's parameter shows a poor correlation with permeability. By using the capillary pressure values in the denominator of Swanson's parameter ($\left(\frac{S_{Hg}}{P_c}\right)_A$), the corresponding pore sizes can be calculated based on the Washburn equation. The Swanson's parameter of samples S1 to S6 corresponds to the pore radii of 8.23, 6.67, 6.68, 5.33, 5.34, and 6.66 μm, respectively. This suggests that only pore radii >5.33 μm contribute to permeability. However, as shown above, pores >0.1 μm contribute significantly to the permeability of coal. As a result, the Swanson's parameter does not correlate well with permeability for coals. *Xiao et al. also found that the Swanson's parameter is not well-correlated with the permeability of tight rocks with complex pore structures because the MIP curves of tight rocks do not produce a characteristic hyperbolic curve, and the Swanson's parameter may not be the inflection point of mercury invasion.*[28]

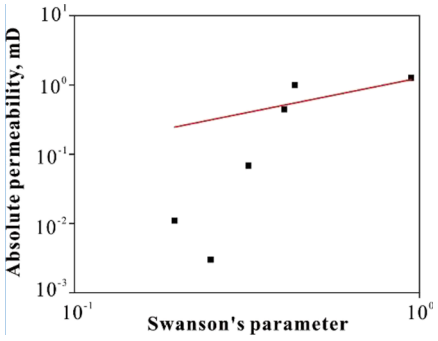

Figure 8. Relationship between permeability and Swanson's parameter.

5.1.3. Purcell Model. Unlike other models that use only one point on the saturation curve for permeability prediction, Purcell relates the permeability to the entire PSD by the assumption of parallel cylindrical capillaries.[4] According to the Purcell model (eq 3), there is a positive linear correlation between permeability and $\varphi \int_0^1 \frac{dS_{Hg}}{P_{ci}^2}$. As shown in Figure 9a, a

https://doi.org/10.1021/acsomega.3c02035
ACS Omega 2023, 8, 21120−21132

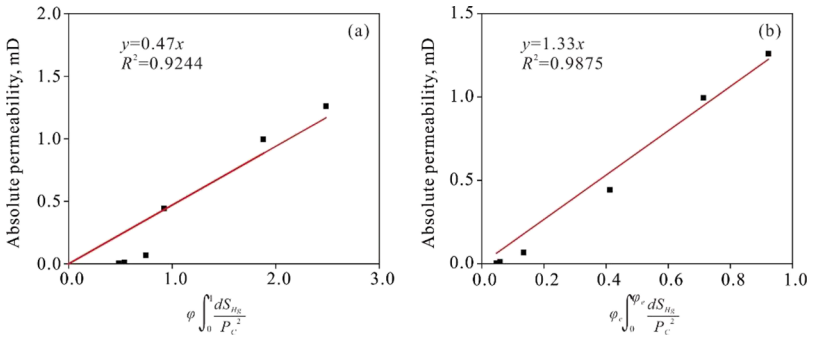

Figure 9. Relationship between permeability and $\varphi \int_0^1 \frac{dS_{Hg}}{P_{ci}^2}$ based on the Purcell model (a); relationship between permeability and $\varphi_e \int_0^{\varphi_e} \frac{dS_{Hg}}{P_{ci}^2}$ based on the modified Purcell model (b).

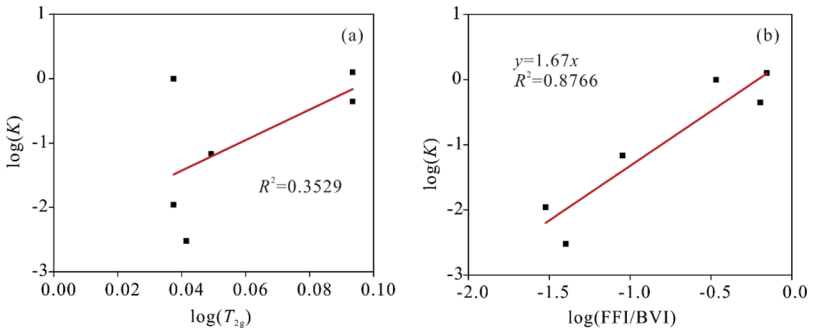

Figure 10. Relationship between log(K) and log(T_{2g}) based on the SDR model (a); relationship between log(K) and log($\frac{FFI}{BVI}$) based on the Coates model (b).

good linear relationship between permeability and $\varphi \int_0^1 \frac{dS_{Hg}}{P_{ci}^2}$ can be found for high-permeability samples (S4, S5 and S6), while the samples with permeability <0.1 mD cannot be fitted by the same linearly relationship. Zhang and Weller also found a poor prediction of low permeability by the Purcell model.[29] They observed that small pores do not contribute to permeability but are considered in the Purcell model. Using a combination of NMR and CT technology, Zhou et al. demonstrated that the large pores (size >0.25 μm in radius) in coal are the main channels for gas flow, accounting for up to 90% of the total volume flux.[50]

5.1.4. The SDR Model. By taking the logarithm of both sides of eq 4, the following expression can be derived:

$$\log K_{SDR} = C_{SDR} + \beta_{SDR} \log \varphi_{NMR} + \alpha_{SDR} \log T_{2gm} \quad (7)$$

Through the correlation analysis between logK_{SDR} and logT_{2gm}, the applicability of SDR model to coal samples can be investigated. Figure 10a shows that there is not a linear correlation between logT_{2gm} and logK_{SDR}, indicating that that the SDR model does not work for coals investigated in this study (Figure 10a). According to Yao et al., the SDR model does not work well for coals because it considers the total porosity, while in fact seepage porosity is far more significant to coal permeability.[16] According to Zheng et al., the SDR model assumes a strong relationship between total porosity and permeability, which is effective for sandstones, but not for the coals.[51]

5.1.5. The Coates Model. Similar to the SDR model, the applicability of Coates model to our studied coal samples can also be investigated by examining the linear relationship between logK_C and log $\frac{FFI}{BVI}$,

$$\log K_C = \beta_C \log \frac{FFI}{BVI} + \frac{\beta_C \alpha_C}{C_C} \log \varphi_{NMR} \quad (8)$$

As shown in Figure 10b, the logK_C show a strong positive correlation with the log $\frac{FFI}{BVI}$ with R^2 = 0.8766, indicating the Coates model is capable of estimating the permeability of coal. Qiao et al. stated that the movable fluid (FFI) located in seepage pores is a key factor in the good performance of the Coates model.[15] It was also found that the estimated permeability shows a strong positive correlation with the measured permeability in the study by Yao et al.[16]

5.2. The Modified Purcell Model. *5.2.1. The Modified Purcell Model Using MIP Result.* As discussed above, the Pittman model and Swanson model poorly predict the permeability of coals because only one pore size is considered. In contrast, the Purcell model and SDR model cannot accurately predict the permeability of low-permeability samples since they use the entire PSD. However, by considering only the connected seepage pores, the Coates model can predict permeability for coals. Since the Purcell model has a strictly theoretical basis, it could be modified to take into account the pore connectivity as well.

The key to modifying the Purcell model lies in selecting a proper pore range. This study focuses on the pore >0.1 mm since pore >0.1 mm in radius account for the bulk of the fluid flow. There are three reasons for the selection of 0.1 μm as the key dimension: (1) previous work has shown that the division between adsorption pores and seepage pores is 0.1 μm, with

https://doi.org/10.1021/acsomega.3c02035
ACS Omega 2023, 8, 21120−21132

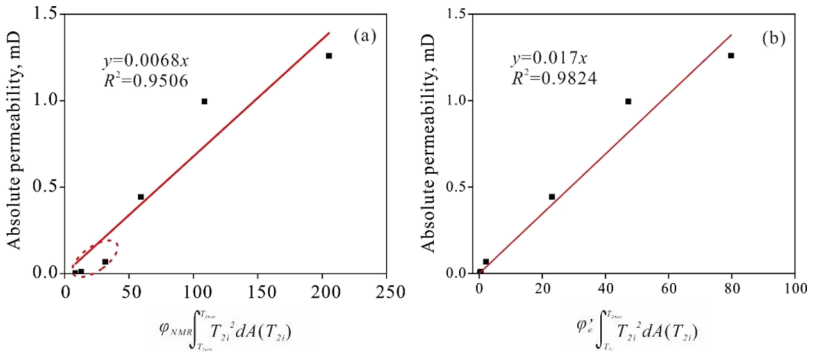

Figure 11. Relationship between permeability and $\varphi_{NMR}\int_{T_{2min}}^{T_{2max}} T_{2i}^2 dA(T_{2i})$ (a); relationship between permeability and $\varphi_e'\int_{T_{2c}}^{T_{2max}} T_{2i}^2 dA(T_{2i})$ (b).

Table 3. Accuracy and Precision of Results of Permeability Models[a]

model	equation	adjusted-R^2	MAE (mD)	MAD (mD)
Pittman model	$\log K_P = 2.1 + 1.4 \log \varphi + 3.1 \log r_{10}$	0.8661	0.13	0.30
Purcell model	$K_{Pu} = 0.47\varphi \int_0^1 \frac{dS_{Hg}}{P_{ci}^2}$	0.9628	0.16	1.23
Modified Purcell model	$K'_{Pu} = 1.33\varphi_e \int_0^{\varphi_e} \frac{dS_{Hg}}{P_{ci}^2}$	0.9926	0.07	0.34
Coates model	$K_C = \left[\left(\frac{\varphi_{NMR}}{0.05}\right)^{0.86} \frac{FFI}{BVI}\right]^{3.60}$	0.8869	0.08	0.44
N−P model	$K_{N-P} = 0.017\varphi_e' \int_{T_{2c}}^{T_{2max}} T_{2i}^2 dA(T_{2i})$	0.9633	0.06	0.10

[a]MAE is mean absolute error, and MAD is maximum absolute deviation.

the former providing the main adsorption space for gas, while the latter provides the principal flow paths.[17,52] (2) NMR data show that the movable water is mainly contained in seepage pores (Figure 5). (3) The fitted result in the Pittman model indicates that pores >0.1 μm are the main contributor to permeability in coals. Therefore, the Purcell model was modified by considering the contribution of different sizes of pores to permeability,

$$K'_{Pu} = 5F(\sigma\cos\theta)^2\varphi_e \int_0^{\varphi_e} \frac{dS_{Hg}}{P_{ci}^2} \quad (9)$$

where φ_e is called effective porosity, defined as the percentage of seepage pores to total pores. As shown in Figure 9b, compared the original model (Figure 9a), the performance of the modified model is significantly enhanced, with a correlation coefficient of 0.9875 between permeability and $\varphi_e \int_0^{\varphi_e} \frac{dS_{Hg}}{P_{ci}^2}$.

5.2.2. The Modified Purcell Model Using NMR Result (N-P Model). Since the PSD obtained from the T_2 spectrum of NMR is related to that obtained from the MIP curve, the NMR T_2 distribution has been used to predict the MIP curves in previous studies.[53,54] Consequently, the NMR T_2 distribution can be used for permeability estimation using the Purcell model.

As discussed in Section 5.1.3, eq 3 shows the relationship between permeability and capillary pressure $K_{Pu} \propto \varphi \int_0^1 \frac{dS_{Hg}}{P_{ci}^2}$. The Washburn equation shows the relationship of the capillary pressure and pore radius:

$$P_c = \frac{2\sigma\cos\theta}{r} \quad (10)$$

Substituting eq 10 in (eq 3), we have

$$K_{Pu} = 5F\varphi \int_0^1 \frac{(\sigma\cos\theta)^2 dS_{Hg}}{P_{ci}^2} = \frac{5}{4}F\varphi \int_{r_{min}}^{r_{max}} r_i^2 dV_{r_i} \quad (11)$$

where V_{r_i} is the volume fraction of pores with the size r_i.

According to the basic principles of NMR, the T_2 relaxation is a function of the radius of pores:[35]

$$\frac{1}{T_2} = \frac{F_s\rho_2}{r} \quad (12)$$

where F_s is the pore shape factor (2 for columnar pores) and ρ_2 is the surface relaxation. The signal amplitude of NMR is proportional to the water content in pores. As a result, V_{r_i} can be expressed as

$$V_{r_i} = CA(T_{2i}) \quad (13)$$

where C is a constant, which is given by the NMR equipment parameter and $A(T_{2i})$ is the NMR signal amplitude at T_{2i} relaxation time.

Substituting eqs 12 and 13 in eq 11, we have

$$K_{N-P} = \frac{5}{4}FF_s\rho_2 C\varphi_{NMR} \int_{T_{2min}}^{T_{2max}} T_{2i}^2 dA(T_{2i}) \quad (14)$$

T_{2C} acts as a separation point between movable and irreducible water. The irreducible fluids are mainly trapped

https://doi.org/10.1021/acsomega.3c02035
ACS Omega 2023, 8, 21120−21132

in adsorption pores, while the movable fluids are stored in seepage pores where they can be easily drained by centrifugation.[17,37] Since the seepage pores account for the vast bulk of the permeability, the equation was modified to consider only these pores,

$$K_{N-P} = \frac{5}{4} FF_s \rho_2 C \varphi_e' \int_{T_{2c}}^{T_{2max}} T_{2i}^{\ 2} dA(T_{2i}) \quad (15)$$

The permeability prediction is poor for low-permeability samples when the new N−P model considers the total porosity (Figure 11a). In contrast, the new N−P model that uses only the seepage porosity has a good fit for all samples (Figure 11b).

5.3. Comparison of Permeability Models. In this study, statistical error analysis was used to compare the permeability models and select the most appropriate one. Different error measurements provide different insights. The adjusted coefficient of determination (R^2_{adj}) is used widely to measure the goodness of a fit,[10] and regression models with different degrees of freedom variables can be compared for the accuracy of the permeability estimation accuracy R^2_{adj}. The mean absolute error (MAE) expresses the average of absolute errors of the predicted data to actual data, while the maximal absolute deviation (MAD) measures the maximum difference between predicted and actual data. The correlated permeability models and the error measures of the permeability models are summarized in Table 3.

Figure 12 shows the correlation between measured permeability and permeability estimated by the various models.

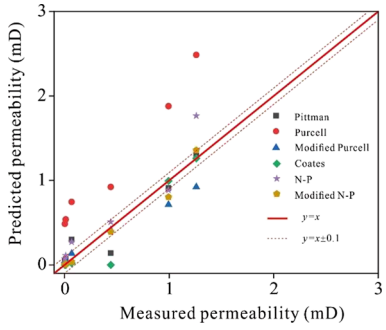

Figure 12. Comparison of the measured air permeabilities and the permeabilities predicted by the models.

The red dashed line identifies the high and low ranges for a difference of 0.1 mD. Although the R^2_{adj} value of the Purcell models is 0.9628, it greatly overestimates the air permeabilities for all samples (the red circles in Figure 12) and has the highest MAE and MAD values (0.16 and 1.23 mD, respectively; Table 3). This is because a significant amount of mercury is injected into the smaller pores of coal samples (Figure 3). These pores do not contribute to permeability but are included in the models for predicting permeability.[29,50] The modified Purcell model provides a very good linear relationship with air permeability (R^2_{adj} = 0.9875), and the MAE and MAD values are extremely low, respectively 0.07 and 0.34 mD (the blue triangles in Figure 12). This model is 50% more accurate than the Purcell model. The Pittman model and Coates model (black rectangles and green diamonds in Figure 12), both empirical models based on sandstone correlations, show good linear relationships with air permeability with R^2_{adj} of 0.8661 and 0.8869, respectively. Both of them have good estimates of air permeability at high permeabilities (>0.5 mD) where MAD <0.1 mD, but show relatively poor performance at low permeabilities (<0.5 mD) where MAD is 0.3 and 0.44 mD, respectively. As reported previously, the poor performance at low permeabilities is because these models assume that porosity and permeability are highly correlated, which is not true for low-permeable coals, where porosity-permeability relationships are weak.[16,23] When all error parameters are combined, the new N−P model provides the best prediction of coal permeability and provides permeability prediction for coal with an accuracy of 0.1 mD (yellow pentagon).

In-situ applications are a potential use of the proposed models, particularly, since NMR analysis can characterize the pore structure and PSD of small, irregularly shaped samples that are difficult to analyze using conventional methods.[47] Consequently, if permeability cannot be directly measured, the pore characteristics can be determined from small samples (such as portions of sidewall core samples or drill cuttings) and used to estimate permeability.

6. CONCLUSIONS

The different models for the prediction of permeability and their applicability to coals have been compared. Based on the Purcell permeability model using MIP data, a new model using NMR data is proposed to estimate the permeability. The following conclusions can be drawn.

(1) Fractal dimension can help to distinguish the interparticle voids filling, intrapore filling, and matrix compression. The influence of interparticle voids and coal compressibility should be carefully examined and corrected before using MIP results to predict coal permeability.

(2) In coals, the bulk of the permeability is contributed by the seepage pores (>0.1 μm), while the contribution of the adsorption pores (<0.1 μm) to permeability is negligible.

(3) The Pittman model and Swanson model, which consider only a single pore size point on the mercury curve, are unsuitable for the prediction of permeability in coals. Additionally, the Purcell and SDR models, which use the entire PSD, fail to predict the permeability of coals when the permeabilities are low.

(4) The Purcell model was modified by considering the specific contribution of different size pores to permeability. The modified model improves the predictive quality by increasing the R^2 and reducing the average absolute error by a factor of approximately 50%.

(5) The modified Purcell model was then applied to NMR data. The coal permeability can be predicted by the new model with an accuracy of 0.1 mD. The model proposed in this paper has the potential to be used in in-situ permeability measurements.

AUTHOR INFORMATION

Corresponding Author

Kun Zhang − *State Key Laboratory of Mining Response and Disaster Prevention and Control in Deep Coal Mines, Anhui University of Science and Technology, Huainan 232001, China;* orcid.org/0000-0002-0076-1139; Email: kzhang@aust.edu.cn

https://doi.org/10.1021/acsomega.3c02035
ACS Omega 2023, 8, 21120−21132

Authors

Yanhai Chang − *State Key Laboratory of Mining Response and Disaster Prevention and Control in Deep Coal Mines, Anhui University of Science and Technology, Huainan 232001, China; China Coal Reservoir Laboratory of National Engineering Research Center of CBM Development & Utilization, China University of Geosciences, Beijing 100083, China;* orcid.org/0009-0005-0201-1453

Yipeng Zhang − *Yangliu Coal Industry Company Limited, Huaibei Mining Group, Huaibei 235000, China*

Complete contact information is available at: https://pubs.acs.org/10.1021/acsomega.3c02035

Notes

The authors declare no competing financial interest.

■ ACKNOWLEDGMENTS

We acknowledge the financial support from the Scientific Research Foundation for High-level Talents of Anhui University of Science and Technology (2022yjrc60) and the National Natural Science Foundation of China (42125205; 42202200).

■ REFERENCES

(1) Wang, C.; Zhao, Y.; Ning, L.; Bi, J. Permeability evolution of coal subjected to triaxial compression based on in-situ nuclear magnetic resonance. *Int. J. Rock Mech. Min. Sci.* **2022**, *159*, No. 105213.

(2) Wang, Z.; Qin, Y.; Shen, J.; Li, T.; Zhang, X.; Cai, Y. A novel permeability prediction model for coal based on dynamic transformation of pores in multiple scales. *Energy* **2022**, *257*, No. 124710.

(3) Laubach, S. E.; Marrett, R. A.; Olson, J. E.; Scott, A. R. Characteristics and origins of coal cleat: A review. *Int. J. Coal Geol.* **1998**, *35*, 175−207.

(4) Rezaee, R.; Saeedi, A.; Clennell, B. Tight gas sands permeability estimation from mercury injection capillary pressure and nuclear magnetic resonance data. *J. Pet. Sci. Eng.* **2012**, *88-89*, 92−99.

(5) Menezes, F. Anisotropy of volume change and permeability evolution of hard sandstones under triaxial stress conditions. *J. Pet. Sci. Eng.* **2019**, *174*, 921−939.

(6) Yang, Z.; Shabani, M.; Solano, N.; Ghanizadeh, A.; Clarkson, C. Experimental determination of gas-water relative permeability for ultra-low-permeability reservoirs using crushed-rock samples: Implications for drill cuttings characterization. *Fuel* **2023**, *347*, No. 128331.

(7) Purcell, W. Capillary pressures-their measurement using mercury and the calculation of permeability therefrom. *J. Pet. Technol.* **1949**, *1*, 39−48.

(8) Swanson, B. A simple correlation between permeabilities and mercury capillary pressures. *J. Pet. Technol.* **1981**, *33*, 2498−2504.

(9) Wells, J., Amaefule, J. Capillary pressure and permeability relationships in tight gas sands. *Paper presented at the SPE/DOE Low Permeability Gas Reservoirs Symposium*, May 19-22, 1985.

(10) Zhao, H.; Ning, Z.; Zhao, T.; Zhang, R.; Wang, Q. Effects of mineralogy on petrophysical properties and permeability estimation of the Upper Triassic Yanchang tight oil sandstones in Ordos Basin Northern China. *Fuel* **2016**, *186*, 328−338.

(11) Li, Y.-H.; Lu, G.-Q.; Rudolph, V. Compressibility and fractal dimension of fine coal particles in relation to pore structure characterization using mercury porosimetry. *Part. Part. Syst. Charact.* **1999**, *16*, 25−31.

(12) Ehrburger-Dolle, F.; Lavanchy, A.; Stoeckli, F. Determination of the surface fractal dimension of active carbons by mercury porosimetry. *J. Colloid Interface Sci.* **2009**, *166*, 451−461.

(13) Yao, Y.; Liu, D. Comparison of low-field NMR and mercury intrusion porosimetry in characterizing pore size distributions of coals. *Fuel* **2012**, *95*, 152−158.

(14) Arns, C.; Knackstedt, M.; Martys, N. Cross-property correlations and permeability estimation in sandstone. *Phys. Rev. E* **2005**, *72*, No. 046304.

(15) Qiao, J.; Zeng, J.; Jiang, S.; Ma, Y.; Feng, S.; Xie, H.; Wang, Y.; Hu, H. Role of pore structure in the percolation and storage capacities of deeply buried sandstone reservoirs: a case study of the Junggar Basin, China. *Mar. Pet. Geol.* **2020**, *113*, No. 104129.

(16) Yao, Y.; Liu, D.; Yao, C.; Tang, D.; Tang, S.; Huang, W. Petrophysical characterization of coals by low-field nuclear magnetic resonance (NMR). *Fuel* **2010**, *89*, 1371−1380.

(17) Cai, Y.; Li, Q.; Liu, D.; Zhou, Y.; Lv, D. Insights into matrix compressibility of coals by mercury intrusion porosimetry and N_2 adsorption. *Int. J. Coal Geol.* **2018**, *200*, 199−212.

(18) Kolodzie, S. Analysis of pore throat size and use of the Waxman-Smits equation to determine OOIP in spindle field, Colorado. *Paper presented at the 1980 Annual Fall Technical Conference of Society of Petroleum Engineers*. Sept. 21-24, 1980.

(19) Pittman, E. Relationship of porosity and permeability to various parameters derived from mercury injection-capillary pressure curves for sandstone. *AAPG Bull.* **1992**, *76*, 191−198.

(20) Rezaee, M. R.; Jafari, A.; Kazemzadeh, E. Relationships between permeability, porosity and pore throat size in carbonate rocks using regression analysis and neural networks. *J. Geophys. Eng.* **2006**, *3*, 370−376.

(21) Ngo, V., Lu, V., Nguyen, M., Hoang, T., Nguyen, H., Le, V. A comparison of permeability prediction methods using core analysis data. *Paper presented at the SPE Reservoir Characterisation and Simulation Conference and Exhibition*, September, 14-16, 2015.

(22) Ngo, V.; Lu, V.; Le, V. A comparison of permeability prediction methods using core analysis data for sandstone and carbonate reservoirs. *Geomech. Geophys. Geo-Energy Geo-Resour.* **2018**, *4*, 129−139.

(23) Liu, K.; Mirzaei-Paiaman, A.; Liu, B.; Ostadhassan, M. A new model to estimate permeability using mercury injection capillary pressure data: application to carbonate and shale samples. *J. Nat. Gas Sci. Eng.* **2020**, *84*, No. 103691.

(24) Guo, B.; Ghalambor, A.; Duan, S. Correlation between sandstone permeability and capillary pressure curves. *J. Pet. Sci. Eng.* **2004**, *43*, 239−246.

(25) Comisky, J., Newsham, K., Rushing, J., Blasingame, T. A comparative study of capillary-pressure-based empirical models for estimating absolute permeability in tight gas sands. *Paper presented at the SPE Annual Technical Conference and Exhibition*; Anaheim, California, USA, November, 11-14, 2007.

(26) Arabjamaloei, R.; Ruth, D. Numerical study of inertial effects on permeability of porous media utilizing the Lattice Boltzmann Method. *J. Nat. Gas Sci. Eng.* **2017**, *44*, 22−36.

(27) Walls, J., Amaefule, J. Capillary pressure and permeability relationships in tight gas sands. *Paper presented at the SPE/DOE Low Permeability Gas Reservoirs Symposium*, May 19-22, 1985.

(28) Xiao, L.; Liu, X.; Zou, C.; Hu, X.; Li, G. Comparative study of models for predicting permeability from nuclear magnetic resonance (NMR) logs in two Chinese tight sandstone reservoirs. *Acta Geophys.* **2014**, *62*, 116−141.

(29) Zhang, Z.; Weller, A. A comparative study of permeability prediction for Eocene sandstones - Part 1: application of modified Swanson models to mercury injection capillary pressure and nuclear magnetic resonance data permeability prediction. *Geophysics* **2021**, *86*, M233−M243.

(30) Timur, A. Pulsed nuclear magnetic resonance studies of porosity, movable fluid, and permeability of sandstones. *J. Pet. Technol.* **1969**, *21*, 775−786.

(31) Daigle, H.; Dugan, B. Extending NMR data for permeability estimation in fine-grained sediments. *Mar. Pet. Geol.* **2009**, *26*, 1419−1427.

(32) Rosenbrand, E.; Fabricius, I. L.; Fisher, Q.; Grattoni, C. Permeability in Rotliegend gas sandstones togas and brine as predicted from NMR, mercury injection and image analysis. *Mar. Pet. Geol.* **2015**, *64*, 189−202.

(33) Guo, J.; Xie, R.; Zou, Y.; Ding, Y. Numerical simulation of multi-dimensional NMR response in tight sandstone. *J. Geophys. Eng.* **2016**, *13*, 285−294.
(34) Maclean, O., James, A., Saleh, J., Hussein, M. Calibration of permeability derived from NMR Logs in Carbonate Reservoirs. *Paper presented at the SPE Middle East Oil Show*; Manama, Bahrain, March 17, 2001.
(35) Coates, G., Xiao, R., Prammer, M. *NMR logging principles and applications*; Gulf Publishing Company: Houston (Texas), 1999.
(36) Lai, J.; Wang, G.; Cao, J.; Xiao, C.; Wang, S.; Pang, X.; Dai, Q.; He, Z.; Fan, X.; Yang, L.; Qin, Z. Investigation of pore structure and petrophysical property in tight sandstones. *Mar. Pet. Geol.* **2018**, *91*, 179−189.
(37) Zheng, S.; Yao, Y.; Liu, D.; Cai, Y.; Liu, Y.; Li, X. Nuclear magnetic resonance T_2 cutoffs of coals: A novel method by multifractal analysis theory. *Fuel* **2019**, *241*, 715−724.
(38) Yao, Y.; Liu, D.; Tang, D.; Tang, S.; Huang, W. Fractal characterization of adsorption−pores of coals from north China: an investigation on CH_4 adsorption capacity of coals. *Int. J. Coal Geol.* **2008**, *73*, 27−42.
(39) Clarkson, C.; Solano, N.; Bustin, R.; Bustin, A.; Blach, T. Pore structure characterization of North American shale gas reservoirs using USANS/SANS, gas adsorption, and mercury intrusion. *Fuel* **2013**, *103*, 606−616.
(40) Friesen, W.; Mikula, R. Mercury porosimetry of coals pore volume distribution and compressibility. *Fuel* **1988**, *67*, 1516−1520.
(41) Yu, Y.; Luo, X.; Wang, Z.; Cheng, M.; Lei, Y.; Zhang, L.; Yin, J. A new correction method for mercury injection capillary pressure (MICP) to characterize the pore structure of shale. *J. Nat. Gas. Sci. Eng.* **2019**, *68*, No. 102896.
(42) Li, K. Analytical derivation of Brooks−Corey type capillary pressure models using fractal geometry and evaluation of rock heterogeneity. *J. Pet. Sci. Eng.* **2010**, *73*, 20−26.
(43) Fu, H. Permeability Prediction of Sandstones Based on Mercury Intrusion Method. *J. Phys.: Conf. Ser.* **2022**, *2152*, No. 012003.
(44) Suuberg, E.; Deevi, S.; Yun, Y. Elastic behaviour of coals studied by mercury porosimetry. *Fuel* **1995**, *74*, 1522−1530.
(45) Toda, Y.; Toyoda, S. Application of mercury porosimetry to coal. *Fuel* **1972**, *51*, 199−201.
(46) Guo, X.; Yao, Y.; Liu, D. Characteristics of coal matrix compressibility: an investigation by mercury intrusion porosimetry. *Energy Fuels* **2014**, *28*, 3673−3678.
(47) Chang, Y.; Yao, Y.; Liu, Y.; Zheng, S. Can cuttings replace cores for porosity and pore size distribution analyses of coal? *Int. J. Coal Geol.* **2020**, *227*, No. 103534.
(48) Yang, Q.; Xue, J.; Li, W.; Du, X.; Ma, Q.; Zhan, K.; Chen, Z. Comprehensive evaluation and interpretation of mercury intrusion porosimetry data of coals based on fractal theory Tait equation and matrix compressibility. *Fuel* **2021**, *298*, No. 120823.
(49) Gao, Z.; Hu, Q. Estimating permeability using median pore-throat radius obtained from mercury intrusion porosimetry. *J. Geophys. Eng.* **2013**, *10*, No. 025014.
(50) Zhou, H. W.; Zhong, J. C.; Ren, W. G.; Wang, X. Y.; Yi, H. Y. Characterization of pore-fracture networks and their evolution at various measurement scales in coal samples using X-ray μCT and a fractal method. *Int. J. Coal Geol.* **2018**, *189*, 35−49.
(51) Zheng, S.; Yao, Y.; Liu, D.; Cai, Y.; Yong, L. Characterizations of full-scale pore size distribution, porosity and permeability of coals: a novel methodology by nuclear magnetic resonance and fractal analysis theory. *Int. J. Coal Geol.* **2018**, *196*, 148−158.
(52) Pan, Z.; Connell, L. D.; Camilleri, M. Laboratory characterisation of coal reservoir permeability for primary and enhanced coalbed methane recovery. *Int. J. Coal Geol.* **2010**, *82*, 252−261.
(53) Volokitin, Y.; Looyestijn, W.; Slijkerman, W.; Hofman, J. A practical approach to obtain primary drainage capillary pressure curves from NMR core and log data. *Petrophysics* **2001**, *42*, 334−343.
(54) Xiao, L.; Mao, Z.; Zou, C.; Jin, Y.; Zhu, J. A new methodology of constructing pseudo capillary pressure (Pc) curves from nuclear magnetic resonance (NMR) logs. *J. Pet. Sci. Eng.* **2016**, *147*, 154−167.

https://doi.org/10.1021/acsomega.3c02035
ACS Omega 2023, 8, 21120−21132